ANNUAL REVIEWS

Annual Review of Biophysics

Prospects and Limitations of High-Resolution Single-Particle Cryo-Electron Microscopy

Ashwin Chari[1] and Holger Stark[2]

[1]Research Group for Structural Biochemistry and Mechanisms, Max-Planck Institute for Multidisciplinary Sciences, Göttingen, Germany

[2]Department of Structural Dynamics, Max-Planck Institute for Multidisciplinary Sciences, Göttingen, Germany; email: hstark1@mpinat.mpg.de

Annu. Rev. Biophys. 2023. 52:391–411

The *Annual Review of Biophysics* is online at biophys.annualreviews.org

https://doi.org/10.1146/annurev-biophys-111622-091300

Keywords

cryo-electron microscopy, macromolecules, protein complexes, 3D structure, optical aberrations, atomic resolution

Abstract

Single particle cryo-electron microscopy (cryo-EM) has matured into a robust method for the determination of biological macromolecule structures in the past decade, complementing X-ray crystallography and nuclear magnetic resonance. Constant methodological improvements in both cryo-EM hardware and image processing software continue to contribute to an exponential growth in the number of structures solved annually. In this review, we provide a historical view of the many steps that were required to make cryo-EM a successful method for the determination of high-resolution protein complex structures. We further discuss aspects of cryo-EM methodology that are the greatest pitfalls challenging successful structure determination to date. Lastly, we highlight and propose potential future developments that would improve the method even further in the near future.

Contents

INTRODUCTION

High-resolution structural information on biological molecules and macromolecular complexes is generally of the utmost interest to understand their function. In the past, the main structure solution methods capable of solving structures at sufficient resolution to allow for atomistic interpretation were X-ray crystallography and nuclear magnetic resonance (NMR). In the past decade, though, a third method, cryogenic electron microscopy (cryo-EM), has matured and become ever more powerful and popular (2). It is now routinely possible to solve structures of biomolecules at high resolution using single-particle cryo-EM (2, 15, 23, 65). This maturation of cryo-EM methodology can be attributed to a series of technological improvements that did not occur instantaneously, but rather in sequential steps (**Figure 1**). Some, such as the construction of better and more automated electron microscopes, are the result of decades-long developments that progressed gradually and at a relatively constant rate. The availability of ever-faster and more powerful computers, using graphical processing unit (GPU) (10, 41, 47, 72) instead of central processing unit (CPU) computing, was also essential to meet the demands imposed by the massive increase in image and particle numbers required for high-resolution structure determination. While some notable high-resolution structures were determined early on using methods including even photographic film and nonautomated image processing procedures (14, 82, 87), a new generation of image processing software was also essential (27, 56, 64, 70, 88). This software has allowed researchers to deal with the (image) data in a more automated manner, allowing less experienced users to determine high-resolution structures without having accumulated years of image processing experience. The replacement of photographic film by a new generation of very powerful direct electron detectors led to a sudden jump in performance (16, 18, 45, 48, 52, 55), and several different detectors became commercially available within a very short time frame. This gave the impression that the impressive improvement in the resolution of cryo-EM structures was solely dependent on the development and availability of these new detectors. While new detector technology certainly would have had some impact on its own, the view that it was the sole factor is perhaps too simplified. One has to emphasize the value of other equally important technological developments in electron microscopic hardware, computation, image processing software, and their respective automation that have contributed to making cryo-EM what it is today. The strength of powerful computers and their ability to cope with more data and more computationally expensive image processing algorithms are also important to underscore in this regard. This

high level of automation in all technological aspects was fundamental for the widespread success of single-particle cryo-EM in the past decade. It also ensures that cryo-EM will remain an invaluable mainstay in the structural biology toolkit.

The massive increase in the performance of cryo-EM has led to the coining of the term resolution revolution (44). Since the start of this revolution, the number of cryo-EM entries in the Electron Microscopy Database (EMDB) has rapidly grown, and the exponential increase in deposited structures has held until today. The growth in deposited structures per year is indeed dramatic, to the extent that cryo-EM has already outperformed NMR in number of yearly depositions and soon can be expected to take over the lead from X-ray crystallography. Apart from the large numbers of solved structures, the highest-attained resolution has also been constantly increasing (**Figure 2**). This shift in maximum resolution can still be understood as the result of ongoing improvements in hardware and software. Even though microscopes and early direct electron detectors were already very good 10 years ago, there was, and still is, sufficient potential for further remarkable improvements in microscopes (61) and detectors (80). In 2021, the first true atomic-resolution structures of apoferritin were published; these structures still mark the current resolution record (59, 81). Improved electron microscopic hardware was used to make both published structures of apoferritin possible.

Although the numbers of determined structures are growing, and the highest attainable resolution keeps improving, not every aspect of development is as impressive. A more detailed look into the statistics of the EMDB (**Figure 2**) reveals that the number of structures in the 3–4 Å regime is growing substantially and steadily. At the same time, it is noteworthy that current statistics from the entire EMDB (not including tomography data) reveal that the average resolution is between 4 and 5 Å; it remains unclear how this will develop in the coming years. This is an unfortunate

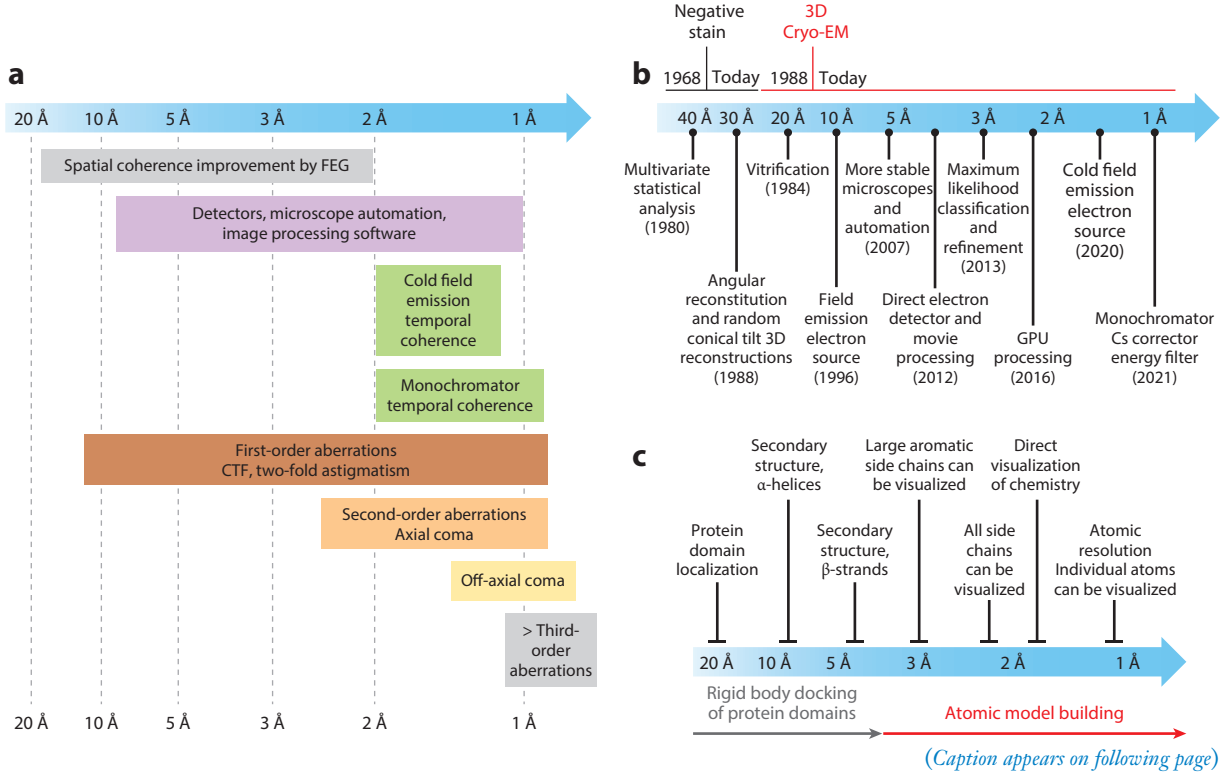

(*Caption appears on following page*)

Figure 1 (*Figure appears on preceding page*)

Importance and timeline of cryogenic electron microscopy (cryo-EM) technical developments and associated achievements. (*a*) Technological developments have differential impact on the ability to attain high resolution in cryo-EM structures. Shown in the horizontal direction from left to right is the increase in resolution; vertical dashed lines mark individual points in the development of resolution to help the reader. Aberrations and the technological developments that correct them do not equally impact all resolution ranges. For example, the improvement of the spatial coherence provided by Shottky field emission guns (FEGs) has impacted resolution ranges from 20 to 2 Å. Developments in detector hardware, microscope automation, image processing software, and correction related to first-order aberrations such as the contrast transfer function (CTF) and twofold astigmatism become important for attaining 10 Å resolution and remain important to achieve resolution better than 1 Å. When attempting to achieve structures in the range of 2 Å to atomic resolution (1.2 Å), the temporal coherence provided by cold field emission sources or a monochromator, as well as the correction of second-order aberrations such as axial coma, becomes essential. When crossing the barrier beyond 1 Å, the temporal coherence provided by a monochromator, the correction of off-axial coma, and even higher-order aberrations becomes indispensable. (*b*) Timeline of technological innovations in cryo-EM technology and the associated resolution barriers that were crossed in structure determination of biological macromolecules. With negatively stained samples in the 1980s, the foundations of multivariate statistical analysis, angular reconstitution, and random conical tilt de novo 3D reconstructions were established. However, negative staining imposed a practical limit in structure determination of approximately 20 Å, which was surpassed by the development of cryo-EM grid preparation procedures by sample vitrification in 1988. The introduction of field emission electron sources in 1996 allowed structures to surpass 10 Å resolution (5). The development of more stable electron microscopes and their automation in 2007 and the introduction of direct electron detectors and movie processing in 2012, maximum likelihood image processing procedures in 2013, and graphical processing unit (GPU)-based image processing in 2016 allowed for the gradual improvement of resolution from 5 to 2 Å. Only in the past two years have either cold field emission electron sources or monochromated electron microscopes equipped with Cs correctors and energy filters allowed for atomic resolution structures of apoferritin to be determined. (*c*) Resolution barriers where structural details in biological macromolecules relevant for functional understanding can be visualized. In resolution ranges from 20 to 10 Å, individual protein domains of known structure can be placed with increasing confidence. Beyond 10 Å resolution, as resolution increases, secondary structures such as, first, individual α-helices and then β-sheets can be localized. At approximately 3 Å resolution, bulky amino acids such as aromatic side chains can be confidently placed. In conjunction with the exhaustive amount of prior knowledge about structures of biological macromolecules, this represents a threshold where the building of atomic models can be initiated. It is not until approximately 2 Å resolution that all amino acids are actually resolved. This also represents a threshold where chemical transformations can be directly visualized and thus directly unequivocally assigned. Individual atoms can only be confidently placed in the structure at resolutions beyond 1.3 Å.

situation because atomic model building is not possible at such resolutions. This obvious discrepancy between the demonstrated technical ability to achieve atomic resolution in some cases and the average of only 4–5 Å resolution for the majority of entries raises a couple of questions that we would like to address in this review. On the one hand, electron microscopic hardware and software is constantly improving, even allowing atomic-resolution structures to be determined. On the other hand, there seem to be limitations for many macromolecular complexes that still prevent structures from reaching resolutions that allow atomic models to be built. It appears likely that these limitations need to be explained by something other than cryo-EM technology.

WHAT ARE THE RESOLUTION-LIMITING FACTORS IN CRYOGENIC ELECTRON MICROSCOPY?

Electron Microscopy Hardware

In general, electron microscopes are by no means diffraction-limited instruments, and, depending on the acceleration voltage, they often have wavelengths far below one-tenth of an Ångström. Electron microscope performance can be severely limited due to mechanical instabilities, vibrations, and thermal drift. This explains why microscopes are usually installed in the basement of a building. Ignoring such problems could render even the most expensive cryo-EM hardware completely useless. In practice, however, it is relatively easy to avoid such limitations even in the preinstallation phase. Most of the hardware-dependent resolution limitations in cryo-EM are thus

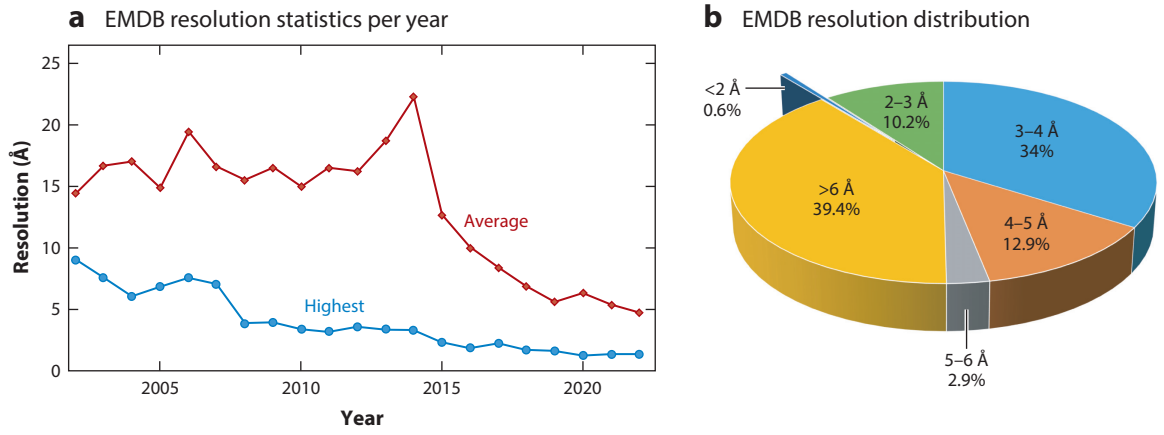

Figure 2

Electron Microscopy Database (EMDB) resolution statistics for single-particle analysis (SPA) entries. (*a*) From all single-particle structure depositions per year in the EMDB, the average (*red*) and highest (*blue*) attained resolutions are plotted. The general trend for both resolution plots indicates a development in the direction of higher resolutions. Notably, the average resolution of single-particle structures deposited to the EMDB lies between 4 and 5 Å. (*b*) Pie chart showing the distribution of structures deposited to the EMDB. Structures with resolutions poorer than 6 Å comprise 39.4%, those between 5–6 Å comprise 2.9%, those between 4–5 Å comprise 12.9%, those between 3–4 Å comprise 34%, those between 2–3 Å comprise 10.2%, and finally structures with resolutions better than 2 Å represent less than 0.6% of all entries.

instead related to lens aberrations (71). Such aberrations depend on the quality of magnetic lenses; the quality of the electron source; the acceleration voltage; and the entire alignment of the optical system, consisting of numerous lenses that have to act together to form a magnified image.

The extent of resolution-limiting aberrations in electron microscopy is often underestimated in cryo-EM because it is highly dependent on the resolution target for which the researchers are aiming. Aberration orders are derived from the wave aberration function (38). Indeed, some higher-order lens aberrations can be totally ignored for certain resolution ranges. The situation, however, changes at higher resolution levels, when an aberration suddenly becomes resolution limiting. To date, most investigations in the cryo-EM field have aimed at resolutions in the range of 2–4 Å. This is sufficient to build atomic models of proteins, but it is also convenient because it allows researchers to entirely ignore some higher-order optical aberrations in current electron microscopes. When we work with any standard cryo-electron microscope in the 2–4 Å resolution range, we can thus indeed afford to almost completely ignore any third- and higher-order lens aberrations. This is different for first-order optical aberrations, such as defocus and twofold astigmatism, and researchers in the field have long accepted that we cannot ignore these in cryo-EM. Instead, we have learned to correct for these aberrations, either by using hardware with a stigmator lens or by mapping different defoci in the x and y directions to a 2D projection image during computational contrast transfer function (CTF) correction (67, 85). There is no way to ignore twofold astigmatism, since it is resolution limiting even in the 5–10 Å resolution regime.

Another higher-order aberration that plays an important role in high-resolution electron microscopy is axial coma (84). Coma is induced by a slight tilt of the beam with respect to the optical axis and causes a phase error in the image. It remained unnoticed for a long time because it only affects high-resolution structure determination. Coma scales with the square of the electron wavelength and the third power of the spatial frequency and remains unnoticed in a power spectrum. While you can ignore the effect of coma completely at approximately 4 Å resolution, it becomes

important at approximately 2 Å and absolutely resolution limiting at 1 Å resolution. The first coma correction strategy was developed in 1978 (84). The so-called Zemlin tableau estimates the level of beam tilt in an image by measuring defocus differences in a series of beam-tilted images (tableau). It is not surprising that coma-free alignments played a large role in high-resolution material science applications, long before it became apparent that they also need to be considered in biological cryo-EM applications. Image acquisition in a coma-free corrected electron microscope was essential for the first high-resolution structure of bacteriorhodopsin (36). Coma plays another important role in current automated data acquisition schemes. To efficiently record large numbers of images in an electron microscope, stage movements have to be minimized because of the time it takes to stabilize the stage after each move (approximately 30 seconds). It has thus become common practice to record several micrographs at the same stage position by using beam and image shift in the electron microscope to cover larger image areas without moving the stage. This image recording strategy, however, introduces coma because of the required beam tilt. Correction of image or beam shift–induced coma during data acquisition was first realized in an electron microscope equipped with a spherical aberration corrector (19). Later, it was also implemented in noncorrected electron microscopes, albeit with lower correction accuracy (see the discussion of Cs correctors below). Recently, methods have also been developed to correct for coma at the image processing level (89).

The number of structures in the EMDB that break the 2 Å resolution barrier is still relatively small, representing 0.6% of all entries (**Figure 2**). Most of these (48%) stem from microcrystal electron diffraction experiments, whereas single-particle cryo-EM structures in that category are currently dominated by apoferritin entries (25%). Nevertheless, these structures demonstrate the feasibility of determining high-resolution and even atomic-resolution structures. They also accentuate the necessity of paying attention to many more aberrations that may become important at 1–1.5 Å or even sub-1 Å resolution. One of these aberrations that has not played any role in structure determination at lower resolution is the off-axial contribution of coma. Even within a single image and in a perfectly coma-free aligned microscope, the amount of coma increases radially from the center of the image out to its edges. In fact, each single electron even adds a coma contribution because of its spiraling trajectory in the microscope, and no software correction exists yet for this type of off-axial coma. Currently, correcting for off-axial aberration (and even higher-order aberrations) by hardware requires a second-generation spherical aberration corrector (57, 81). Whereas the first corrector generation (CETCOR) (58) had two hexapole lenses to correct for spherical aberration, the second generation (BCOR) uses three hexapoles to also correct for off-axial contributions. This minimizes off-axial coma to an extent that imaging can be considered coma free even at the sub-1 Å level over the entire field of view (57, 81).

At the 1 Å level, chromatic aberration also becomes a highly resolution-limiting factor. For a long time, the cryo-EM field was happy with the improvement in the coherence of the electron beam caused by the change from thermionic electron sources to field emission sources in the 1990s (83). In field emission sources, the spatial and temporal coherence increased substantially; this was another major contribution to microscope development that made the cryo-EM resolution revolution possible (**Figure 1**). Initially, field emission electron sources became interesting mainly because of their increase in spatial coherence, which plays a major role in single-particle imaging at relatively strong defocus values up to several micrometers. The improved temporal coherence was not considered to be important because limitations caused by chromatic aberration did not become apparent at resolutions attained in structures at the time. Most installed high-end cryo-electron microscopes use a thermally assisted Schottky field emission design with an energy spread of 0.7–0.8 eV. Such electron sources have approximately 85% signal transfer at 2 Å

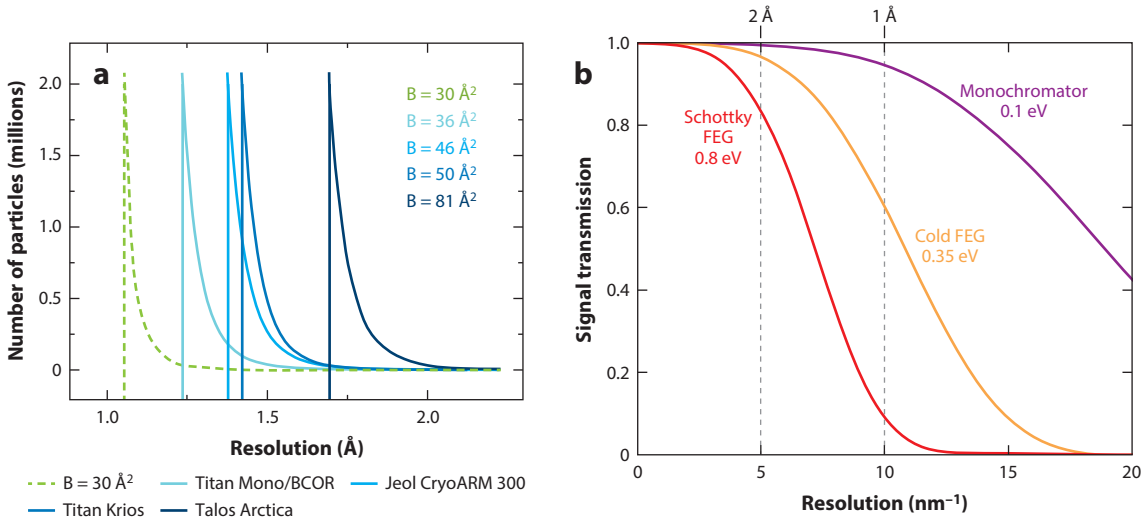

Figure 3

The limitations imposed by cryogenic electron microscopy (cryo-EM) hardware performance are hard physical limits. (*a*) Experimental B-factors, as defined by the Rosenthal & Henderson plot (68), result in hard resolution limits for a given cryo-EM imaging system. The explosive nature of the required particle numbers at high resolution becomes more readily apparent when B-factors are displayed in a linear plot. Note the similar performance of the various microscope systems for apoferritin structures at resolutions up to 2 Å. The B-factor of 36 Å^2 obtained for the Krios Mono/BCOR indicates that particle numbers will become prohibitive when attempting to attain structures slightly better than 1.25 Å. A microscope or detector setup that could break the 1 Å resolution barrier with acceptable particle numbers and, consequently, beam time needs to have a B-factor of <30 Å^2. (*b*) The resolution-dependent dampening of the signal for different electron sources due to chromatic aberration calculated for a Titan Krios C_{Twin} objective lens with a chromatic aberration coefficient of 3.26 mm (relativistically corrected to 300 kV; 29). For simplicity, two dashed vertical lines indicate 2 and 1 Å resolution, respectively. The thermally assisted Shottky field emission design (*red*) with an energy spread (equivalent to chromatic aberration) of approximately 0.8 eV has a signal transfer of greater than 80% at 2 Å resolution, but the signal would be dampened to less than 10% at 1 Å. The situation becomes better with a cold field emission gun (FEG) (*orange*) that has an energy spread of only approximately 0.35 eV. In this case, only 40% signal dampening would occur at 1 Å resolution without significant loss at 2 Å resolution. A monochromator (*purple line*), taking the increased chromatic aberration (3.8 mm) due to the BCOR into account, reduces the energy spread further, to approximately 0.1 eV. The use of a monochromator is therefore required when aiming at structure determination with <1 Å resolution.

resolution (**Figures 2** and **3**). So-called cold field emission sources are technically more difficult to realize but have an improved energy spread of only 0.35 eV, which implies that the signal loss in the image due to chromatic aberration is expected to be much smaller than that in Schottky field emission (31). In fact, in the 1–2 Å resolution regime, cold field emission sources can provide much more signal compared to Schottky field emission sources (40, 59) (**Figures 2** and **3**). The dampening of high-resolution signals in most currently installed microscopes may thus explain the relatively small percentage of structures at <2 Å resolution in the database. In a Schottky field emission microscope, the signal at 1 Å resolution is already reduced to approximately 10%, whereas the cold field emission microscope will still retain approximately 60% of the signal. At 1.5 Å and beyond, chromatic aberration thus becomes extremely resolution limiting for the majority of today's high-end microscopes equipped with Schottky field emission. The smallest energy spread to date can be realized by a monochromator, which can reduce the energy spread down to 0.1 eV. This increase in temporal coherence over all other electron sources makes it much more powerful in the very-high-resolution range (better than 1.5 Å). In such a monochromated microscope, the signal at 1 Å is only dampened by approximately 10%. This is comparable to the optical

performance of a cold field emission microscope at 2 Å resolution. Breaking the 1 Å resolution barrier in cryo-EM is thus most likely to be achieved with a monochromated electron microscope, but it will remain a challenging goal for several other reasons that are not related to instrumentation (see below). Currently, there is only one monochromated cryo-electron microscope installed worldwide (81), and one can thus consider the current fleet of high-end electron microscopes to be optically suitable to 1.5 Å resolution if the sample itself allows such resolutions to be obtained.

The current commercially available high-end electron microscopes are equipped with 300 kV cold field emission electron sources, an energy filter, and an electron-counting direct electron detector optimized for this high voltage. One can, however, argue whether this is the best optical design for a microscope that is supposed to deliver data in the 3 Å range. According to Peet et al. (63), the ideal acceleration voltage with optimal signal transfer and minimum beam damage should be 100 kV. Such a 100-kV microscope has already been shown to be good enough to provide structures at resolutions allowing atomic model building (61). However, much greater investment by the microscope manufacturers will be needed to build an 100-kV cryo-electron microscope with a large detector optimized to work at 100 kV, a field emission electron source, and an automatic sample loader to become competitive with the current 200 kV and 300 kV electron microscopes.

Electron Detectors

The first generation of direct electron detectors for cryo-EM became available in 2012 (9) and outperformed photographic film and charge-coupled device cameras. These detectors also transformed the way in which data are recorded and processed today. Instead of a single image, the micrograph consists of a series of movie frames, which was immediately recognized to be beneficial for single-particle cryo-EM (6, 9, 26, 86). The image frames can be aligned to each other and, thus, allow correction of any beam-induced motion in the images. While not all images in cryo-EM suffer from significant motion blur, it is still very common, and the ability to correct for this motion had a massive impact on the productivity of cryo-EM. Another positive aspect of the direct electron detectors is that the electron dose is fractionated, which allows users to adjust the final dose in the computed 3D reconstruction and therefore mitigate radiation damage (26). Movie frames with high accumulated electron dose can be skipped entirely, or their high-resolution signal can be down-weighted (6, 67, 86). Even zero-dose extrapolation has been suggested (60). Whether this indeed will become routinely possible in the future will depend on understanding all sources and the extent of errors in the electron optics and the image analysis tools that we apply. There is no doubt that these detectors are key to the widespread success of cryo-EM. Currently, there are already third- and fourth-generation cameras available, and the improvements in detector quantum efficiency and speed are remarkable from one generation to another (53). A perfect detector still remains out of reach, but future improvements can be expected, although they will likely become more incremental. Commercially available detectors that we use in high-end microscopes today differ from each other in many aspects, but the choice of detector does not critically influence protein structure determination.

Image Processing

Before the resolution revolution, image processing of cryo-EM data required extensive knowledge of modularized image processing packages such as SPIDER (21), IMAGIC (78), and later EMAN (49) and XMIPP (51). Use of these programs required long training, numerous manual steps, and adjustments of many parameters. This situation has changed completely; the most commonly used

software packages for single-particle cryo-EM are now RELION (70) and CryoSPARC (64), both of which provide an advanced level of automation and automated parameter adjustments. Iterative 3D classification and refinement algorithms are based on maximum likelihood principles (74), which avoid major user bias and overfitting problems. High-resolution structure determination in cryo-EM is therefore mostly under the control of the software itself. This allows cryo-EM image processing newcomers to determine a high-resolution structure from a good image test data set within a few hours. Some preprocessing of the data, such as movie frame alignment of the images and CTF parameter estimation, is required. Once a 3D structure has been determined, these parameters can be refined, which normally provides another improvement in resolution (88).

As mentioned above, higher-order aberrations such as coma need to be taken into account when aiming for high resolution. Some computational tools have been developed in recent years to account for beam tilt–induced coma in the images (89) and also for the defocus variations within the z dimension of the imaged molecules themselves. The latter is also known as Ewald sphere correction (69).

Atomic-Resolution Structure Determination

The first true atomic-resolution 3D reconstructions of a protein, apoferritin, became available only recently (59, 81). Two different electron microscopes were used, and both used better optics than the majority of currently installed high-end microscopes. One microscope, based on a Titan Krios G4, was equipped with a cold field emission electron source, an energy filter, and a Falcon 4 electron detector (ThermoFisher). The other microscope, a prototype based on a Titan Krios G3 (ThermoFisher), had a monochromator in combination with a second-generation spherical aberration corrector (BCOR, CEOS GMBH, Heidelberg) and a Falcon 3 electron detector. Thus, both microscopes had an electron source with a smaller energy spread than that of the majority of high-end microscopes, leading to a better signal transfer of high-resolution information (below 2 Å). This is highly relevant for atomic-resolution structure determination because chromatic aberration becomes a major limiting factor at this resolution (**Figure 4**). The energy filter has another clear effect on image quality, since the same resolution of apoferritin can be obtained from a smaller number of particle images when recorded in energy-filtered mode (59). Only one of the instruments is equipped with a spherical aberration corrector (81). This BCOR corrector has three hexapole lenses, in contrast to the first-generation CETCOR corrector, which has only two hexapoles. The CETCOR corrector was developed for material science applications and revealed a considerable amount of off-axis coma over the larger field of view that is typical for biological applications. The third hexapole lens in the BCOR spherical aberration corrector is used to keep the off-axial coma almost 10 times lower than in a normal Titan Krios. An electron microscope with a BCOR can thus be considered as a fully aplanatic optical system (57). The benefit of using this corrector for high-resolution cryo-EM is that coma can be minimized very efficiently by accurately tuning the corrector. Both axial and off-axial coma contributions thus become negligible, and high-resolution 3D structures can be determined without the need for beam-tilt correction using software. Another advantage of the BCOR is that large image shifts are still compatible with coma-free imaging. For example, coma is kept to such low values that aberration-free imaging below 1 Å is achievable even at image shifts up to 10 μm. This optical precision and accuracy cannot be obtained with any normal, noncorrected electron microscope.

Atomic-resolution structure determination from data recorded without a BCOR corrector, therefore, will always require an additional beam-tilt parameter to be estimated, and corrected for, during image processing. While this indeed can be done in RELION (89), one needs to consider that this adds another fitted parameter to image processing for which the extent of introduced

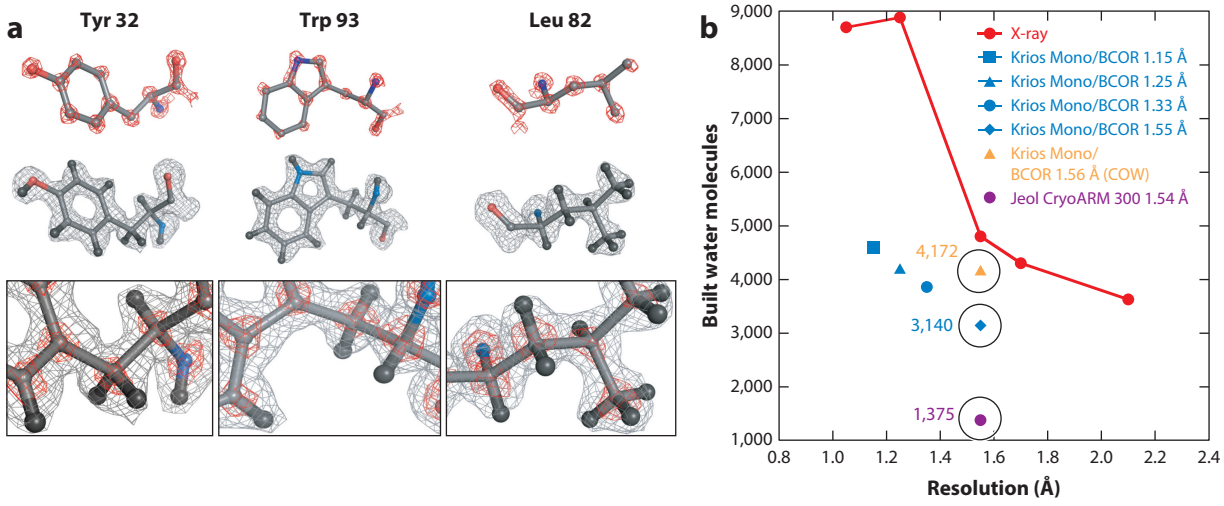

Figure 4

Atomic-resolution structure determination of apoferritin by cryogenic electron microscopy (cryo-EM) and map quality estimation. (*a*) Shown are excerpts from the 1.25 Å resolution structure of apoferritin. In high thresholded maps (*red mesh*), the densities for individual atoms become discernable (*top*). At lower map thresholds (*gray mesh*), bumps become visible that are consistent with the positions of hydrogen atoms (*middle*). The bottom panels depict the same excerpts with high (*red mesh*) and low (*gray mesh*) threshold maps overlaid. (*b*) Inspection of the solvent region in high-resolution cryo-EM density maps may allow the definition of structure quality metrics. The plot depicts the number of water molecules in various apoferritin structures in the ordinate axis versus attained resolution of the structure in the abscissa axis. In addition, the number of water molecules found in various X-ray structures (*red dots*) are compared to those that could be placed confidently in cryo-EM maps using the identical strategy and threshold cutoffs (Krios Mono/BCOR RELION in blue, Krios Mono/BCOR COW in orange, and Jeol in magenta). At 1.5 Å resolution, substantially more water molecules were identified for two reconstructions using different software from apoferritin recorded in the Krios Mono/BCOR microscope compared to an apoferritin structure determined at very similar nominal resolution with data recorded in a high-end Jeol (CryoARM 300) microscope. The highest number of water molecules could be confidently placed in a 1.56 Å structure that was calculated with the COW software. For this model, the number of placed water molecules is close to an X-ray crystal structure at this resolution. It is noteworthy that the number of water molecules that were located in the X-ray structures is still generally higher than for cryo-EM maps, and determining higher-resolution cryo-EM structures does not significantly increase the number of water molecules that can be unequivocally modeled, for reasons that are currently unknown.

errors is unknown. Especially for atomic resolution, structure determination errors become very crucial because we want to model and interpret all map details directly as chemical information. This is different from reconstructions at lower resolution (approximately 3 Å), for which we mostly use the prior knowledge available from chemical information to aid in atomic model building. Smaller errors in the map therefore do not matter to the same extent at 3 Å resolution as at <1.5 Å resolution. Working at atomic resolution with cryo-EM (or any other structure determination method) thus only makes sense if we can trust all details in the map sufficiently to allow reliable and trustworthy interpretation of the deviations from normal chemistry. High-resolution cryo-EM structures that lack this required precision and quality are a waste of the effort needed to attain resolutions higher than 2 Å.

Resolution Versus Quality

In cryo-EM, the resolution is estimated by the correlation of information in Fourier shells (32). The currently widely accepted resolution threshold is defined as the point where the correlation of Fourier space shells in two independently reconstructed maps from half data sets drops

below 0.143. Mathematically, the Fourier shell correlation (FSC) represents a measure of self-consistency, and it can only be expanded to estimate resolution under the assumption that both half data sets are completely independent from each other. Any dependence between the two half data sets would result in a correlation signal that does not carry structural information. If this happens, then the FSC no longer estimates resolution only, but also estimates other sources of correlating information. By definition, systematic errors in the data or data processing will be present in both half data sets. The half data sets are thus no longer independent and also generate correlations that misestimate the resolution of the reconstructed structure. Simulations have shown that, when images suffer from coma or from errors in coma correction, the FSC will show an increase in correlation, resulting in a misestimation of the resolution of the structure (7). Such a resolution misestimation will not contribute any additional information that can be utilized to interpret the structure. When aiming for higher and higher resolution in cryo-EM, we have to exert caution in not overemphasizing the FSC as a sole criterion. Otherwise, because of the many possibilities in polishing a FSC curve, it could become a scoring function that users might be able to misuse.

As mentioned above, the effort necessary to determine atomic-resolution structures is only warranted when every single atom position can be visualized and interpreted with high confidence. This allows for direct and accurate chemical interpretation of the map and would put us in a position where we can fully trust every individual atom in the resulting atomic model. It might seem that a single atom and its placement with high accuracy are not terribly important in a structure consisting of several tens of thousands of atoms. However, it should be emphasized that high-resolution protein structure determination is highly relevant for structure-based drug design. In this regard, when it comes to the accurate placement of small effectors and the inference of chemical inhibition mechanisms from structural data, precise positioning of a single atom can make all the difference. This was shown, for example, by improvements in the resolution of the human 20S proteasome structure from 2.6 Å (33) to 1.8 Å resolution (73). This allowed Schrader et al. (73) to determine that the inhibition with epoxyketone-class inhibitors results in the formation of a 7-ring covalent linkage, in contrast to a 6-ring linkage, as was previously reported (28). The difference between these two covalent linkages in the structure was only one atom (out of approximately 26,000) and led to a redefinition of the inhibition mechanism of the 20S proteasome. Thus, although the difference is only one atom, it is highly relevant for the $20 billion annual market share that is occupied by proteasome inhibitors in cancer treatments (42).

The FSC does not provide any quality indicators for high-resolution reconstructions. Especially at very high and atomic resolutions, quality becomes a major issue influencing the interpretation of chemical details in a protein. What other possible standards exist to judge the quality of a 3D map? Even if some high-resolution structures (1.5 Å resolution) of the same complex have been reported, the maps are likely to differ in quality for many reasons. A sensitive way to compare map quality is to inspect the solvent region more closely (81). Solvent densities are weaker, noisier, and thus potentially better reporters for map quality than the protein itself. A comparison of three 1.5 Å resolution apoferritin maps with data from different microscopes and structures reconstructed using different software revealed interesting insights when water molecules were modeled using the same criterion in all of the maps (**Figure 4**). Even though all of these apoferritin structures are among the best-quality maps within the EMDB, they still differ significantly by almost a factor of three in the number of water molecules that could be confidently modeled in the different structures. Two observations are interesting within this context: First, the number of water molecules identified reliably in the cryo-EM maps was always lower than for X-ray structures at comparable resolution. Second, the number of water molecules was strongly dependent not only on the microscope but also on the software that was used for

image processing and the final map refinement. Thus, especially when it comes to structure-based drug design and the deciphering of chemical mechanisms from protein structures, not only are the electron optical details of a microscope important, but also how the data is processed. The solvent regions in high-resolution cryo-EM 3D maps may therefore offer future opportunities to develop methods for quantitative analysis of their quality.

Where Is the Resolution Limit in Single-Particle Cryo-Electron Microscopy?

Cryo-EM is now able to determine the structure of apoferritin even at atomic resolution. This may raise the question of how far the resolution limit of cryo-EM can be pushed in the future. This is of course a multifactorial problem that depends on the microscope, the detectors, the sample, and the image processing software. Resolution limits can be gauged by a single parameter that considers the entire chain of samples, imaging, and computation simultaneously. The Rosenthal & Henderson plot (68) is a very useful tool that serves this purpose very well. The plot shows how particle image numbers (on a logarithmic scale) correlate with the achieved resolution (by $1/\text{resolution}^2$). This relationship is linear, and from the determined slope, one calculates a so-called experimental B factor. A high B factor indicates that more particles are needed to calculate a given 3D structure. However, it provides no information about the source of the problem. When we consider the best and most rigid sample (apoferritin) and keep data processing procedures constant, the B factor will report only about the utilized microscope–detector combination (81). From such B factor plots, we thus obtain information about the regime in which certain microscope–detector combinations are useful (**Figure 3**). The B factor will also inform us about the limitations of a given microscope–detector combination because we can extrapolate how many particles would be required from a given set of hardware to determine higher-resolution structures. The B factors of all of the currently installed and available microscopes indeed reveal that all commercially available microscope–detector combinations are good enough to determine 3D structures in the 2–3 Å range. For the very best microscope, this will require much less beam time and thus fewer particle statistics, and for all other cryo-EM hardware, this would also be practically achievable and will not require unreasonable amounts of time for data collection.

This changes, however, at very high and atomic resolutions, where small differences in B factors can have tremendous influence on the maximum resolution that can be attained. A high-end cryo-electron microscope therefore makes the most sense when aiming for atomic resolution because, with cheaper and less sophisticated microscope setups, such resolutions in structures are out of reach (**Figure 3**). Should the user be happy with 3 Å reconstructions, there is clearly no need to buy the most expensive microscope.

Even the current best microscopes would struggle to improve the resolution of apoferritin to significantly better than 1 Å. The reason for this is that 1,000,000 particles were already used for the first atomic-resolution structure determination. At this number of images, the microscope is already operating in a regime where the B factor plot indicates prohibitive outcomes (**Figure 3**). Adding another few million particle images would not bring considerably improved resolution. In addition, it is an oversimplification to extrapolate numbers of particles from a B factor plot to obtain higher resolution because it requires the inherent assumption that the optical performance of the microscope does not deteriorate at higher resolution. As demonstrated above, due to the resolution dampening effect of chromatic and other aberrations, such extrapolations can fail easily (**Figure 3**). A Rosenthal & Henderson plot can only provide a good estimate for the number of particles required to reach higher resolution if the optical performance of the microscope and that of the detector are the same and if the high-resolution signal is not hampered by any other hardware parameter.

Based on these considerations, it is currently hard to imagine 1 Å resolution cryo-EM structures being elucidated routinely. Current microscopes are not capable of working productively in that regime, and an additional problem is that B factors for samples other than apoferritin are considerably higher. However, one can expect that, in the future, next-generation microscopes will enable more frequent structure determination at resolutions in the 1.5 Å regime. Breaking the 1 Å resolution barrier seems currently to be still out of reach for proteins other than apoferritin.

Samples and Biochemistry

The statistics of the EMDB clearly reveal that the resolution mean of current depositions is not in the very-high-resolution range (**Figure 2**). The mean resolution value has undoubtedly improved over the past six years, but it is still above 4 Å, even though there is some high-resolution bias in the EMDB from the many high-resolution apoferritin and ribosome structures. Considering the experimental B factors of current microscope–detector combinations, electron microscopic hardware is not the key factor limiting the mean resolution value to 4 Å; in fact, the hardware should enable values better than 3 Å. The current difficulties in reaching higher resolution for some samples should thus be attributed to factors other than electron microscopic hardware and image processing software; the other most likely source of difficulties is the sample itself.

Macromolecular complexes can be quite diverse in many aspects. They vary significantly in size, cellular abundance, symmetry, rigidity, and stability. Some complexes are relatively easy to purify, while others pose major challenges in biochemical purification. Space constraints do not allow us to elaborate on the intricacies of recombinant expression, extraction from exogenous and endogenous sources, and the myriad of purification technologies. The interested reader is, however, referred to several excellent publications and reviews on these topics (1, 3, 4, 8, 20, 34, 50, 54, 66, 77, 79). In this section, we focus solely on aspects that we consider to be of outstanding importance to the determination of high-resolution cryo-EM structures. Very often, the quality of single particles revealed by cryo-EM images does not keep up with the expectations raised by common biochemical analysis. Some complexes can indeed readily dissociate and are not stable over time. There is also a tendency for many complexes to aggregate, which could be a result of dissociation or degradation occurring during purification (**Figure 5**). Another likely explanation for bad behavior in cryo-EM could be the choice of buffer systems (12) (**Figure 6**). It is rare that purification protocols are optimized for maximal structural integrity of the complex, and sample aggregation is known to be strongly influenced by pH. A few tools have been developed to improve this situation. ProteoPlex (12) is a sensitive thermal melting method to screen for stabilizing buffer conditions of a purified complex with relatively small demands in terms of sample amounts. One of the main outcomes of using ProteoPlex is that the two highest probabilities for stabilizing any given complex are at pH 6.5 and pH 8, strikingly contrasting with the strong pH 7.5 preference in the EMDB (**Figure 6**).

One of the often-cited advantages of cryo-EM over both X-ray crystallography and NMR is that low amounts of protein and no crystals are required for structure determination. As a matter of fact, the lower amount of required sample can indeed be an important advantage, as shown by the numerous structures that have been determined in recent years. One should, however, not neglect the fact that low protein concentrations are not always an advantage. A potential danger of working with dilute samples lies in the labile interactions among subunits of protein complexes. Weak binding affinities could result in spontaneous dissociation of protein components when working at the concentrations required for cryo-EM, resulting in aggregation or structural heterogeneity as a consequence of stochastic subunit dissociation. Likewise, the employment of tags for purification is well-documented to impact the composition and relative stoichiometries of subunits of macromolecular complexes (30, 46). Some complexes can be dissociated or degraded even by standard

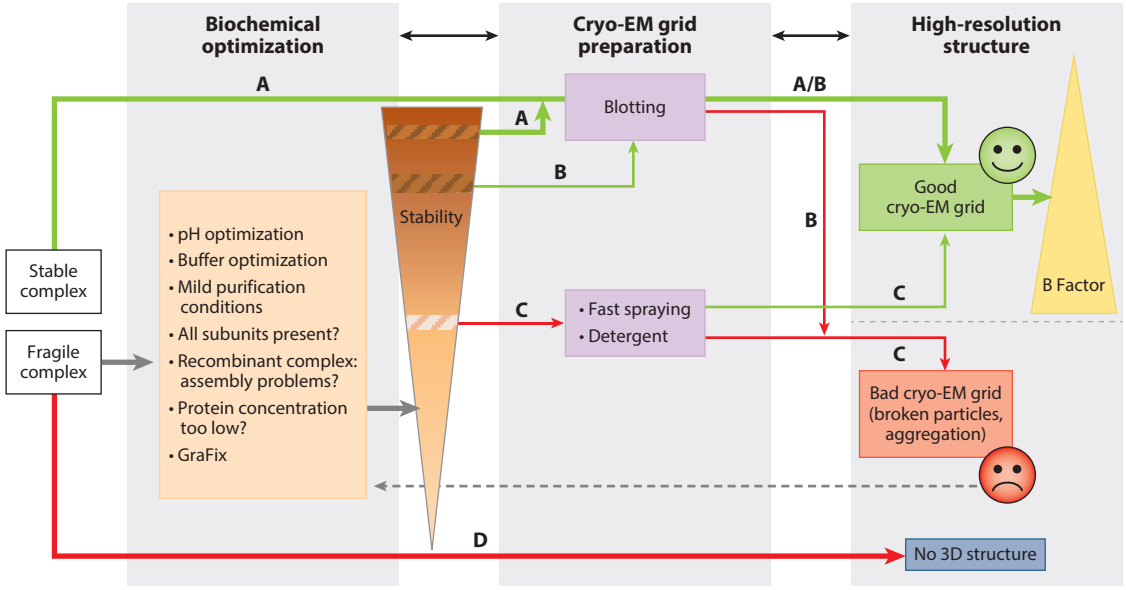

Figure 5

Biochemical sample quality affects the Rosenthal & Henderson B factor plot (68), cryogenic electron microscopy (cryo-EM) productivity, and the ability to determine high-resolution structures. Stable complexes, as described in this review for apoferritin and fatty acid synthase (FAS) containing the γ-subunit, withstand blotting-based cryo-EM grid preparation procedures and allow for high-resolution structure determination (route A). The B factor for these samples is solely dependent on electron microscopic hardware and the sample conformational space. Some samples, however, such as FAS prepared by our chromatography-free procedures, are partially dissociated or destabilized by blotting-based grid preparation procedures. Such samples will benefit from fast spraying or the inclusion of detergents when preparing cryo-EM grids (route B). Biochemically fragile complexes will entirely resist cryo-EM grid preparation, and in these cases, structure determination will become impossible due to dissociation, destabilization, or aggregation of the sample (route D). In these latter cases, even fast-spraying cryo-EM grid preparation or the use of detergent will not be sufficient to obtain images of intact particles (route C). As illustrated in this review for FAS with a bound γ-subunit, biochemical optimization of sample stability by some of the strategies mentioned in the beige box is essential for preparing good cryo-EM grids by conventional blotting procedures, use of detergents, or fast-spraying methods. Irrespective of the exact nature of cryo-EM grid preparation procedures, biochemical optimization has the huge benefit of reducing the B factor of the Rosenthal & Henderson plot. This is well-documented to increase cryo-EM productivity (by reducing beam time) and the possibility of elucidating high-resolution structures (by reducing the number of required particles).

biochemical purification procedures (37 and references therein). These dissociating or degrading factors can arise through biochemical constraints imposed by the chromatographic technique for binding and elution, which may well lie outside of the stability window of the macromolecular complex in question (12), or the sieving effect exerted by chromatographic supports (39). In some cases, the interaction affinity of some subunits with supports and nonspecific surfaces can exceed their affinity for other subunits of the cognate macromolecular complex (22). This has a profound impact on the stability of complexes over the course of purification, but also on blotting procedures in cryo-EM grid preparation (see the section titled The Air–Water Interface). Some of these destabilized or dissociated complexes may be salvaged, for example, by mild chemical fixation and subsequent size fractionation (76). However, entirely avoiding subunit dissociation or destabilization appears preferable for two reasons. First, assembly of macromolecular complexes often utilizes intricate pathways in cellulo to avoid misassembly, kinetic traps in assembly, and the formation of dead-end near-cognate nonfunctional complexes (11, 35). Second, the responsible assembly chaperones are not present in purified systems, causing dissociation to be irreversible and

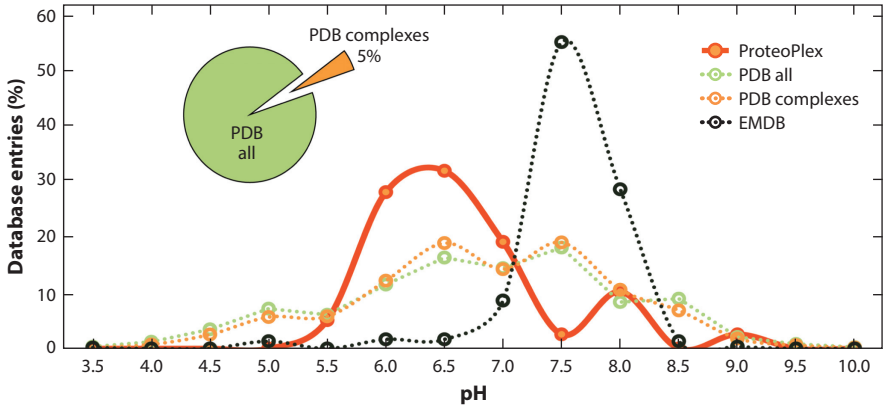

Figure 6

pH distribution of structures in the Protein Data Bank (PDB) and the Electron Microscopy Database (EMDB). Plotted are the percentual distribution of entries in the *y* axis against pH values in which the structures were determined in the *x* axis (the plot was generated in 2015 and considers entries up to that year). The green dotted line represents all PDB entries, while the orange dotted line represents only structures of complexes within the PDB. As shown in the pie chart, the entries for complexes in the PDB comprise 5% of all entries. There is no distinction between all PDB entries and PDB macromolecular complex entries, which both show a broad pH distribution. In contrast, the majority of EMDB structures are determined at a pH of 7.5 (*black dotted line*). The distribution of all optimized pH values, as determined by ProteoPlex, is also shown (*bold orange line*). It displays biphasic behavior of stability, with one phase centered at pH 6.5 and the other centered at pH 8.0. Most complexes are unstable at pH 7.5, unlike at the pH values used for most electron microscopy structure determination projects.

leading to the determination of nonfunctional, off-pathway structures. A profound consequence of stochastic subunit dissociation or destabilization is that one would remain entirely unable to even recognize that one has lost an integral subunit (75). This is a particularly dangerous scenario because the only readout would be a badly behaving protein complex where grid preparation and either structure determination altogether or attainment of high resolution fail for nonapparent reasons (**Figure 5**).

The Air–Water Interface

Protein complex purification is a delicate biochemical task and requires dedication to a degree that is often underestimated; more emphasis is placed on discussing how the process of grid preparation itself might dissociate or destabilize samples (17, 24, 25, 43). It has been shown by systematic tomographic analysis that proteins do not swim freely in solution but actually concentrate at the air–water interface (AWI) (62). The AWI is considered to be a hostile environment for proteins that can lead to (partial) denaturation, which in turn would explain why many proteins look so bad in cryo-EM (17). Denaturation at the AWI has become a widely accepted assumption in the cryo-EM community. However, it is important to note that, to date, no direct observations of protein denaturation at the AWI exist. It is in fact extremely difficult to distinguish denaturation from disintegration. There is clear experimental evidence that binding particles to a support film (17), adding detergent to a solution (13), or freezing protein complexes at a speed that does not allow the proteins to move to the AWI (43) can sometimes mitigate the observed adverse behavior of a protein on a cryo-EM grid (**Figure 5**). However, in spite of these advances in mitigating the effects of the AWI, considerable difficulties still exist in preparing cryo-EM grids of monodisperse and stable protein complexes. Consequently, for these protein complexes, it is unlikely that

high-resolution structure determination ever will be possible. Cryo-EM productivity would be greatly enhanced if the source of difficulties in preparing grids were to be understood and the problems solved (**Figure 5**).

Considering the importance attributed to the AWI for preparing high-quality cryo-EM grids, it is surprising that there currently is only one published systematic investigation, dealing with the yeast fatty acid synthase (FAS) (17). This study appears to support the idea of denaturation by showing in a series of experiments that FAS is dissociated or destabilized when located at the AWI. This detrimental effect on FAS integrity and stability can be minimized when FAS is bound to a graphene film. A frequently disregarded aspect in this context is that several potentially dissociating or destabilizing surface interactions are encountered by the sample in the course of biochemical purification, as mentioned above. Most importantly, samples always encounter the AWI when eluted as droplets from columns or when fractionated from density gradients; however, in cryo-EM, we believe that these encounters are only deleterious while preparing grids. This assumption appears flawed considering that we are unable to estimate the degree of dissociation or destabilization occurring in biochemical purification. In particular, regulatory subunits are inherently weak binders that can easily be lost during purification. Confounding the issue, tools to measure and validate the well-being of a given macromolecular complex at each stage of biochemical purification remain entirely elusive. Thus, rather than solely invoking the role of the AWI, it appears more productive to suppose that a combination of biochemical principles might contribute to the negative outcomes of cryo-EM grid preparation.

Singh et al. (75) recently purified FAS, making use of a completely different purification strategy that entirely avoids chromatographic steps and instead relies on precipitation and density gradient centrifugation steps alone. Even though FAS has been intensively investigated for six decades, they discovered an additional, previously overlooked subunit that was dissociated in the course of purification by virtue of its weak binding affinity in earlier studies. Consequently, all structural and functional work has to date been done with an incomplete yeast FAS lacking this γ-subunit that modulates and fine-tunes its activity. Singh et al. found that the presence of this subunit stabilizes FAS to an extent that they could no longer observe the dissociation or destabilization found by D'Imprima et al. (17), which amounted to 90% of all FAS particles. Purification of FAS with Singh et al.'s newly developed purification strategy and certifiably removing this novel γ-subunit by virtue of genetic deletion changed this ratio, and they saw only 40% damaged particles. This calls the postulated physical denaturing of FAS at the AWI into question, as this denaturing should result in exactly the same degree of dissociation irrespective of the purification procedure. Adding the γ-subunit back to this FAS preparation had a dramatic effect, entirely preventing dissociation or destabilization related to cryo-EM grid preparation. This effect caused by the γ-subunit is surprising, as it binds in the inner cavity of FAS and is therefore never exposed to the AWI. For FAS, we can thus indeed conclude that the absence of a previously unknown subunit resulted in biochemical destabilization, rendering the complex susceptible to damage at the AWI. Thus, the logical consequence from these data is that forces exerted at the AWI are sufficient to disintegrate the complex. Using biochemically optimized FAS, we have also recently been able to elucidate a cryo-EM structure at 1.9 Å resolution with our monochromated and Cs corrected Titan Krios microscope. Combining the effects of biochemical sample optimization and microscope hardware did result in a significantly improved B factor for FAS imaging that is compatible with even higher-resolution structure determination in the future. In conclusion, biochemical dissociation or destabilization of protein complexes in protein purification cannot be categorically excluded and seems to be somewhat underestimated in the cryo-EM field. When AWI-related issues in cryo-EM grid preparation become apparent, it might be an indication for the biochemist

that not everything is completely under control. Improved biochemical purification strategies with minimized risk for dissociation and other strategies that can either stabilize complexes or reduce the destabilizing effects of the AWI should therefore be combined to make cryo-EM an even more productive and effective technique. This can be combined with other strategies like fast spraying or adding detergents to ameliorate cryo-EM grid preparation and thus make those complexes accessible to high-resolution structure determination by cryo-EM (**Figure 5**).

SUMMARY AND OUTLOOK

Current cryo-EM equipment is already fully compatible with high-resolution structure determination. However, at very high resolution, some optical and technical challenges have yet to be overcome. Extrapolations from the current state-of-the-art microscope optics and detector technology indicate that breaking the 1 Å resolution barrier in single-particle cryo-EM should not be expected to happen routinely. However, cryo-EM hardware and software are compatible with routine structure determination at <2 Å resolution. In reality, however, such resolutions can currently only be attained for some extremely stable, well-behaved, and homogeneous complexes.

There still is ample scope for the development of better biochemical procedures for the purification and stabilization of macromolecular complexes. The increase in the number of structures at resolutions <2 Å in the database will be aided by improvements in electron microscopic hardware but will mainly require overcoming the current challenges and problems of cryo-EM sample preparation. Improved grid preparation and vitrification procedures, combined with the already existing improvements in electron microscopic hardware, would allow us to solve more macromolecular complex structures at high resolution using cryo-EM in the future. These developments have to move alongside the definition of quality metrics, which validate that high-resolution cryo-EM maps are able to unequivocally place single atoms with high precision and accuracy. This will undoubtedly include the ability to estimate how errors arise in every step of structure determination by cryo-EM and how these errors propagate in subsequent steps until the final structure is determined.

DISCLOSURE STATEMENT

The authors are not aware of any affiliations, memberships, funding, or financial holdings that might be perceived as affecting the objectivity of this review.

LITERATURE CITED

1. Almo SC, Garforth SJ, Hillerich BS, Love JD, Seidel RD, Burley SK. 2013. Protein production from the structural genomics perspective: achievements and future needs. *Curr. Opin. Struct. Biol.* 23:335–44
2. Bai XC, McMullan G, Scheres SHW. 2015. How cryo-EM is revolutionizing structural biology. *Trends Biochem. Sci.* 40:49–57
3. Barford D, Takagi Y, Schultz P, Berger I. 2013. Baculovirus expression: tackling the complexity challenge. *Curr. Opin. Struct. Biol.* 23:357–64
4. Berger I, Fitzgerald DJ, Richmond TJ. 2004. Baculovirus expression system for heterologous multiprotein complexes. *Nat. Biotechnol.* 22:1583–87
5. Bottcher B, Wynne SA, Crowther RA. 1997. Determination of the fold of the core protein of hepatitis B virus by electron cryomicroscopy. *Nature* 386:88–91
6. Brilot AF, Chen JZ, Cheng AC, Pan JH, Harrison SC, et al. 2012. Beam-induced motion of vitrified specimen on holey carbon film. *J. Struct. Biol.* 177:630–37

7. Bromberg R, Guo Y, Borek D, Otwinowski Z. 2019. High-resolution cryo-EM reconstructions in the presence of substantial aberrations. bioRxiv 798280. **https://doi.org/10.1101/798280**
8. Byrne B. 2015. *Pichia pastoris* as an expression host for membrane protein structural biology. *Curr. Opin. Struct. Biol.* 32:9–17
9. Campbell MG, Cheng A, Brilot AF, Moeller A, Lyumkis D, et al. 2012. Movies of ice-embedded particles enhance resolution in electron cryo-microscopy. *Structure* 20:1823–28
10. Castano-Diez D, Moser D, Schoenegger A, Pruggnaller S, Frangakis AS. 2008. Performance evaluation of image processing algorithms on the GPU. *J. Struct. Biol.* 164:153–60
11. Chari A, Fischer U. 2010. Cellular strategies for the assembly of molecular machines. *Trends Biochem. Sci.* 35:676–83
12. Chari A, Haselbach D, Kirves JM, Ohmer J, Paknia E, et al. 2015. ProteoPlex: stability optimization of macromolecular complexes by sparse-matrix screening of chemical space. *Nat. Methods* 12:859–65
13. Chen J, Noble AJ, Kang JY, Darst SA. 2019. Eliminating effects of particle adsorption to the air/water interface in single-particle cryo-electron microscopy: bacterial RNA polymerase and CHAPSO. *J. Struct. Biol. X* 1:100005
14. Chen JZ, Settembre EC, Aoki ST, Zhang X, Bellamy AR, et al. 2009. Molecular interactions in rotavirus assembly and uncoating seen by high-resolution cryo-EM. *PNAS* 106:10644–48
15. Cheng YF. 2015. Single-particle cryo-EM at crystallographic resolution. *Cell* 161:450–57
16. Clough R, Kirkland AI. 2016. Direct digital electron detectors. *Adv. Imaging Electron Phys.* 198:1–42
17. D'Imprima E, Floris D, Joppe M, Sanchez R, Grininger M, Kuhlbrandt W. 2019. Protein denaturation at the air-water interface and how to prevent it. *eLife* 8:e42747
18. Faruqi AR, Henderson R. 2007. Electronic detectors for electron microscopy. *Curr. Opin. Struct. Biol.* 17:549–55
19. Fischer N, Neumann P, Konevega AL, Bock LV, Ficner R, et al. 2015. Structure of the *E. coli* ribosome-EF-Tu complex at <3 Å resolution by Cs-corrected cryo-EM. *Nature* 520:567–70
20. Forler D, Kocher T, Rode M, Gentzel M, Izaurralde E, Wilm M. 2003. An efficient protein complex purification method for functional proteomics in higher eukaryotes. *Nat. Biotechnol.* 21:89–92
21. Frank J, Shimkin B, Dowse H. 1981. SPIDER—a modular software system for electron image processing. *Ultramicroscopy* 6:343–57
22. Gavin AC, Bosche M, Krause R, Grandi P, Marzioch M, et al. 2002. Functional organization of the yeast proteome by systematic analysis of protein complexes. *Nature* 415:141–47
23. Glaeser RM. 2019. How good can single-particle cryo-EM become? What remains before it approaches its physical limits? *Annu. Rev. Biophys.* 48:45–61
24. Glaeser RM, Han B-G. 2017. Opinion: hazards faced by macromolecules when confined to thin aqueous films. *Biophys. Rep.* 3:1–7
25. Glaeser RM, Han B-G, Csencsits R, Killilea A, Pulk A, Cate JHD. 2016. Factors that influence the formation and stability of thin, cryo-EM specimens. *Biophys. J.* 110:749–55
26. Grant T, Grigorieff N. 2015. Measuring the optimal exposure for single particle cryo-EM using a 2.6 Å reconstruction of rotavirus VP6. *eLife* 4:e06980
27. Grant T, Rohou A, Grigorieff N. 2018. *cis*TEM, user-friendly software for single-particle image processing. *eLife* 7:e35383
28. Groll M, Kim KB, Kairies N, Huber R, Crews CM. 2000. Crystal structure of epoxomicin:20S proteasome reveals a molecular basis for selectivity of α′,β′-epoxyketone proteasome inhibitors. *J. Am. Chem. Soc.* 122:1237–38
29. Haider M, Muller H, Uhlemann S, Zach J, Loebau U, Hoeschen R. 2008. Prerequisites for a Cc/Cs-corrected ultrahigh-resolution TEM. *Ultramicroscopy* 108:167–78
30. Hakhverdyan Z, Domanski M, Hough LE, Oroskar AA, Oroskar AR, et al. 2015. Rapid, optimized interactomic screening. *Nat. Methods* 12:553–60
31. Hamaguchi T, Maki-Yonekura S, Naitow H, Matsuura Y, Ishikawa T, Yonekura K. 2019. A new cryo-EM system for single particle analysis. *J. Struct. Biol.* 207:40–48
32. Harauz G, van Heel M. 1986. Exact filters for general geometry three dimensional reconstruction. *Optik* 73:146–56

33. Harshbarger W, Miller C, Diedrich C, Sacchettini J. 2015. Crystal structure of the human 20S proteasome in complex with carfilzomib. *Structure* 23:418–24
34. Hart DJ, Waldo GS. 2013. Library methods for structural biology of challenging proteins and their complexes. *Curr. Opin. Struct. Biol.* 23:403–8
35. Hayer-Hartl M, Hartl FU. 2020. Chaperone machineries of Rubisco—the most abundant enzyme. *Trends Biochem. Sci.* 45:748–63
36. Henderson R, Baldwin JM, Downing KH, Lepault J, Zemlin F. 1986. Structure of purple membrane from *Halobacterium halobium*—recording, measurement and evaluation of electron micrographs at 3.5 Å resolution. *Ultramicroscopy* 19:147–78
37. Henneberg F, Chari A. 2021. Chromatography-free purification strategies for large biological macromolecular complexes involving fractionated PEG precipitation and density gradients. *Life* 11:1289
38. Hosokawa F, Sawada H, Kondo Y, Takayanagi K, Suenaga K. 2013. Development of Cs and Cc correctors for transmission electron microscopy. *Microscopy* 62:23–41
39. Jungbauer A, Machold C, Hahn R. 2005. Hydrophobic interaction chromatography of proteins—III. Unfolding of proteins upon adsorption. *J. Chromatogr. A* 1079:221–28
40. Kato T, Makino F, Nakane T, Terahara N, Kaneko T, et al. 2019. The 1.54 Å resolution structure of apoferritin by CRYOARM300 with Cold-FEG. *Microsc. Microanal.* 2(Suppl.):998–99
41. Kimanius D, Forsberg BO, Scheres SHW, Lindahl E. 2016. Accelerated cryo-EM structure determination with parallelisation using GPUs in RELION-2. *eLife* 5:e18722
42. Kisselev AF. 2022. Site-specific proteasome inhibitors. *Biomolecules* 12:54
43. Klebl DP, Monteiro DCF, Kontziampasis D, Kopf F, Sobott F, et al. 2020. Sample deposition onto cryo-EM grids: from sprays to jets and back. *Acta Crystallogr. D* 76:340–49
44. Kuhlbrandt W. 2014. The resolution revolution. *Science* 343:1443–44
45. Kuijper M, van Hoften G, Janssen B, Geurink R, De Carlo S, et al. 2015. FEI's direct electron detector developments: embarking on a revolution in cryo-TEM. *J. Struct. Biol.* 192:179–87
46. LaCava J, Molloy KR, Taylor MS, Domanski M, Chait BT, Rout MP. 2015. Affinity proteomics to study endogenous protein complexes: pointers, pitfalls, preferences and perspectives. *Biotechniques* 58:103–19
47. Li XM, Grigorieff N, Cheng YF. 2010. GPU-enabled FREALIGN: accelerating single particle 3D reconstruction and refinement in Fourier space on graphics processors. *J. Struct. Biol.* 172:407–12
48. Li XM, Mooney P, Zheng S, Booth CR, Braunfeld MB, et al. 2013. Electron counting and beam-induced motion correction enable near-atomic-resolution single-particle cryo-EM. *Nat. Methods* 10:584–90
49. Ludtke SJ, Baldwin PR, Chiu W. 1999. EMAN: semiautomated software for high-resolution single-particle reconstructions. *J. Struct. Biol.* 128:82–97
50. Maeda S, Schertler GFX. 2013. Production of GPCR and GPCR complexes for structure determination. *Curr. Opin. Struct. Biol.* 23:381–92
51. Marabini R, Masegosa IM, San Martin MC, Marco S, Fernandez JJ, et al. 1996. Xmipp: an image processing package for electron microscopy. *J. Struct. Biol.* 116:237–40
52. McMullan G, Faruqi AR, Clare D, Henderson R. 2014. Comparison of optimal performance at 300keV of three direct electron detectors for use in low dose electron microscopy. *Ultramicroscopy* 147:156–63
53. McMullan G, Faruqi AR, Henderson R. 2016. Direct electron detectors. *Methods Enzymol.* 579:1–17
54. Mesa P, Deniaud A, Montoya G, Schaffitzel C. 2013. Directly from the source: endogenous preparations of molecular machines. *Curr. Opin. Struct. Biol.* 23:319–25
55. Milazzo AC, Cheng AC, Moeller A, Lyumkis D, Jacovetty E, et al. 2011. Initial evaluation of a direct detection device detector for single particle cryo-electron microscopy. *J. Struct. Biol.* 176:404–8
56. Moriya T, Saur M, Stabrin M, Merino F, Voicu H, et al. 2017. High-resolution single particle analysis from electron cryo-microscopy images using SPHIRE. *J. Vis. Exp.* 123:55448
57. Muller H, Massmann I, Uhlemann S, Hartel P, Zach J, Haider M. 2011. Aplanatic imaging systems for the transmission electron microscope. *Nucl. Instrum. Methods Phys. Res. A* 645:20–27
58. Muller H, Uhlemann S, Hartel P, Haider M. 2008. Aberration-corrected optics: from an idea to a device. In *Proceedings of the 7th International Conference on Charged Particle Optics (CPO-7), Cambridge, United Kingdom, July 24–26*, Vol. 1, pp. 167–78. Red Hook, NY: Curran Assoc.
59. Nakane T, Kotecha A, Sente A, McMullan G, Masiulis S, et al. 2020. Single-particle cryo-EM at atomic resolution. *Nature* 587:152–56

60. Naydenova K, Jia P, Russo CJ. 2020. Cryo-EM with sub-1 Å specimen movement. *Science* 370:223–26
61. Naydenova K, McMullan G, Peet MJ, Lee Y, Edwards PC, et al. 2019. CryoEM at 100 keV: a demonstration and prospects. *IUCrJ* 6:1086–98
62. Noble AJ, Dandey VP, Wei H, Braschi J, Chase J, et al. 2018. Routine single particle CryoEM sample and grid characterization by tomography. *eLife* 7:e34257
63. Peet MJ, Henderson R, Russo CJ. 2019. The energy dependence of contrast and damage in electron cryomicroscopy of biological molecules. *Ultramicroscopy* 203:125–31
64. Punjani A, Rubinstein JL, Fleet DJ, Brubaker MA. 2017. cryoSPARC: algorithms for rapid unsupervised cryo-EM structure determination. *Nat. Methods* 14:290–96
65. Renaud JP, Chari A, Ciferri C, Liu WT, Remigy HW, et al. 2018. Cryo-EM in drug discovery: achievements, limitations and prospects. *Nat. Rev. Drug Discov.* 17:471–92
66. Rigaut G, Shevchenko A, Rutz B, Wilm M, Mann M, Seraphin B. 1999. A generic protein purification method for protein complex characterization and proteome exploration. *Nat. Biotechnol.* 17:1030–32
67. Rohou A, Grigorieff N. 2015. CTFFIND4: fast and accurate defocus estimation from electron micrographs. *J. Struct. Biol.* 192:216–21
68. Rosenthal PB, Henderson R. 2003. Optimal determination of particle orientation, absolute hand, and contrast loss in single-particle electron cryomicroscopy. *J. Mol. Biol.* 333:721–45
69. Russo CJ, Henderson R. 2018. Ewald sphere correction using a single side-band image processing algorithm. *Ultramicroscopy* 187:26–33
70. Scheres SHW. 2012. RELION: implementation of a Bayesian approach to cryo-EM structure determination. *J. Struct. Biol.* 180:519–30
71. Scherzer O. 1936. Over some errors of electron lenses. *Z. Phys.* 101:593–603
72. Schmeisser M, Heisen BC, Luettich M, Busche B, Hauer F, et al. 2009. Parallel, distributed and GPU computing technologies in single-particle electron microscopy. *Acta Crystallogr. D* 65:659–71
73. Schrader J, Henneberg F, Mata RA, Tittmann K, Schneider TR, et al. 2016. The inhibition mechanism of human 20S proteasomes enables next-generation inhibitor design. *Science* 353:594–98
74. Sigworth FJ. 1998. A maximum-likelihood approach to single-particle image refinement. *J. Struct. Biol.* 122:328–39
75. Singh K, Graf B, Linden A, Sautner V, Urlaub H, et al. 2020. Discovery of a regulatory subunit of the yeast fatty acid synthase. *Cell* 180:1130–43.e20
76. Stark H. 2010. GraFix: stabilization of fragile macromolecular complexes for single particle cryo-EM. *Methods Enzymol.* 481:109–26
77. Stark H, Chari A. 2016. Sample preparation of biological macromolecular assemblies for the determination of high-resolution structures by cryo-electron microscopy. *Microscopy* 65:23–34
78. Vanheel M, Keegstra W. 1981. IMAGIC—a fast, flexible and friendly image analysis software system. *Ultramicroscopy* 7:113–30
79. Vijayachandran LS, Viola C, Garzoni F, Trowitzsch S, Bieniossek C, et al. 2011. Robots, pipelines, polyproteins: enabling multiprotein expression in prokaryotic and eukaryotic cells. *J. Struct. Biol.* 175:198–208
80. Vinothkumar KR, Henderson R. 2016. Single particle electron cryomicroscopy: trends, issues and future perspective. *Q. Rev. Biophys.* 49:e13
81. Yip KM, Fischer N, Paknia E, Chari A, Stark H. 2020. Atomic-resolution protein structure determination by cryo-EM. *Nature* 587:157–61
82. Yu X, Jin L, Zhou ZH. 2008. 3.88 A structure of cytoplasmic polyhedrosis virus by cryo-electron microscopy. *Nature* 453:415–19
83. Zemlin F, Beckmann E, van der Mast KD. 1996. A 200 kV electron microscope with Schottky field emitter and a helium-cooled superconducting objective lens. *Ultramicroscopy* 63:227–38
84. Zemlin F, Weiss K, Schiske P, Kunath W, Herrmann KH. 1978. Coma-free alignment of high resolution electron microscopes with the aid of optical diffractograms. *Ultramicroscopy* 3:49–60
85. Zhang K. 2016. Gctf: real-time CTF determination and correction. *J. Struct. Biol.* 193:1–12
86. Zheng SQ, Palovcak E, Armache JP, Verba KA, Cheng YF, Agard DA. 2017. MotionCor2: anisotropic correction of beam-induced motion for improved cryo-electron microscopy. *Nat. Methods* 14:331–32

87. Zhou ZH. 2011. Atomic resolution cryo electron microscopy of macromolecular complexes. *Adv. Protein Chem. Struct. Biol.* 82:1–35
88. Zivanov J, Nakane T, Forsberg BO, Kimanius D, Hagen WJH, et al. 2018. New tools for automated high-resolution cryo-EM structure determination in RELION-3. *eLife* 7:e42166
89. Zivanov J, Nakane T, Scheres SHW. 2020. Estimation of high-order aberrations and anisotropic magnification from cryo-EM data sets in *RELION*-3.1. *IUCrJ* 7:253–67